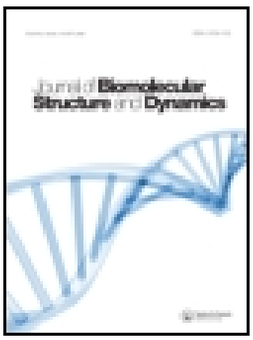

Taylor & Francis
Taylor & Francis Group

Journal of Biomolecular Structure and Dynamics

ISSN: 0739-1102 (Print) 1538-0254 (Online) Journal homepage: https://www.tandfonline.com/loi/tbsd20

Investigation on the fungicide resistance mechanism against *Botrytis cinerea* β-tubulin inhibitor zoxamide by computational study

Songjie Du, Kun Zhang, Xiaojun Yao & Juan Du

To cite this article: Songjie Du, Kun Zhang, Xiaojun Yao & Juan Du (2019): Investigation on the fungicide resistance mechanism against *Botrytis cinerea* β-tubulin inhibitor zoxamide by computational study, Journal of Biomolecular Structure and Dynamics, DOI: 10.1080/07391102.2019.1671230

To link to this article: https://doi.org/10.1080/07391102.2019.1671230

Accepted author version posted online: 21 Sep 2019.
Published online: 03 Oct 2019.

JOURNAL OF BIOMOLECULAR STRUCTURE AND DYNAMICS
https://doi.org/10.1080/07391102.2019.1671230

Taylor & Francis
Taylor & Francis Group

LETTER TO THE EDITOR

Investigation on the fungicide resistance mechanism against *Botrytis cinerea* β-tubulin inhibitor zoxamide by computational study

Songjie Du[a], Kun Zhang[a], Xiaojun Yao[b] and Juan Du[a]

[a]Shandong Province Key Laboratory of Applied Mycology, College of Life Science, Qingdao Agricultural University, Qingdao, China; [b]College of Chemistry and Chemical Engineering, Lanzhou University, Lanzhou, China

Communicated by Ramaswamy H. Sarma

ARTICLE HISTORY Received 16 July 2019; *a*ccepted 17 September 2019

Introduction

Botrytis cinerea, a polyphagous plant pathogen, causes the plant gray mold by the parasitic way of necrotrophic nutrition, which infects more than 200 species of plants, and seriously damages the most of economic crops, including vegetable and fruit, ornamental flowers, grain, and so on (Wang et al., 2019). Gray mold brings out the annual economic losses of 10 to 100 billion dollars in worldwide, which increased the burden of realizing the agricultural industry anticipated development (Negri et al., 2017). In terms of economic impact, *Botrytis cinerea* has been considered one of the top 10 most important phytopathogens (Dean et al., 2012). Furthermore, it is the most common pathogen causing decay during pre- and post-harvesting and storing of crops. As a matter of fact, the biological interaction between *Botrytis cinerea* with host is intricate. Using spores with small size and light weight, *Botrytis cinerea* attacks the diverse plant hosts by variety of the infection strategies, in which the main processes are penetrating the host tissue, secreting enzymes and toxins to destroy the normal metabolism of the cells (Van Kan, 2006). *Botrytis cinerea* is difficult to control due to the following characteristics, including the wide range of hosts, high environmental fitness of spores and long infection of time, which has developed into an urgent problem to be solved (Van Kan, 2006).

A series of prevention and control measures have been employed in China against the gray mold, some of which have developed comparatively complete systems. The measures with manner of ecofriendly and sustainability, including some biological and agricultural approaches, were used to control *Botrytis cinerea*, while those were not sufficient for desired effect. Based on that, controlling of gray mold mainly rely on chemical approach currently, and it plays an important role relying on its advantage of high efficiency and labor-saving (Wang et al., 2019). However, the same fungicide was used intensively and continuously, which increases the risk of resistance in the *Botrytis cinerea*.

One of the targets of chemical fungicide is *Bc*β-tubulin, which polymerizes with α-tubulin to form microtubules. Microtubules are one of the cytoskeleton components and play important roles in many processes, such as supporting cell structure and cell division. Currently, the fungicides, benzimidazole and benzamide are available to control gray mold, while *Botrytis cinerea* have appeared resistance to these fungicides. According to experimental verification (Leroux et al., 2002), the reason of drug-resistance is that *Bc*β-tubulin has occurred single base pair mutations. The mutated position at codons 198 and 200 are related to benzimidazoles resistance (Leroux et al., 2002). Another fungicide zoxamide (Zox, Figure 1), belonging to the benzamide, has unique physiological activity against oomycetes, which is the only registered fungicide for the control of oomycete pathogen in some economic crop (Young & Slawecki, 2001). The interaction mode of zoxamide is similar to that of benzimidazole, but the resistance mechanism has not been well understood. The amino acids of β-tubulin substitutions resulting in benzimidazole (E198A, F200Y) resistance have been detected. According to reports (Adnan, Hamada, Li, & Luo, 2018), the E198V mutation is not directly involved in the interaction modes of β-tubulin and zoxamide, so it makes little difference on zoxamide-resistance. Cai et al. found that *Botrytis cinerea* is resistant to zoxamide, which is associated with mutations of F200Y or M233I (Cai et al., 2015). Met233, considered as the unique target site for binding zoxamide, has an impact on the function of β-tubulin, which may be linked to the different frequency resistance of zoxamide relative to benzimidazoles (Cai et al., 2015). It is not well understood that the resistance mechanism against Zox at atomic level.

Computational methods, such as molecular docking, molecular dynamics simulation, etc. have been successfully applied in the study of drug or pesticide resistance mechanism (Wu et al., 2018; Zhu & Yang, 2012). In this study, we select the *Bc*β-tubulin (wild type protein and mutant protein) and the fungicide zoxamide as object to investigate the interaction

CONTACT Juan Du dujuannx@126.com Shandong Province Key Laboratory of Applied Mycology, College of Life Science, Qingdao Agricultural University, Changcheng Road 700#, Qingdao, 266109 China

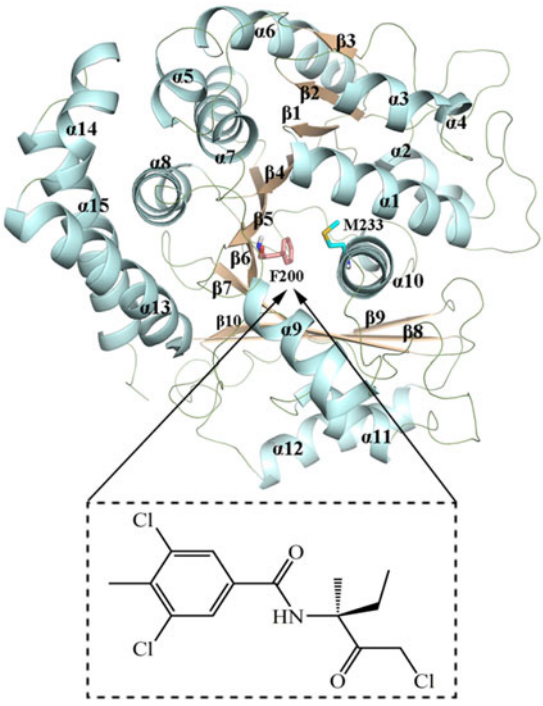

Figure 1. The three-dimensional structure of Βcβ-tubulin and the structure of Zox. The mutant sites with F200, M233 are shown as pink and light blue sticks. α-helix, β-sheet, loop are colored in palecyan, wheat and palegreen, respectively.

mode between them and resistance mechanism of *Botrytis cinerea* against Zox, using multiple computational methods, for instance, homology modeling, molecular docking, molecular dynamics simulation, residue interaction network analysis and binding free energy calculation. Zox was docked to the binding pocket of *Bc*β-tubulin^{WT}. Based on the docking results, the complex of β-tubulin^{F200Y}-Zox and β-tubulin^{M233I}-Zox were constructed. 100 ns molecular dynamics simulations were performed on the systems of WT, F200Y and M233I in complex with Zox. Molecular Mechanics Generalized Born Surface Area and Poisson-Boltzmann Surface Area (MM-GB/PBSA) methods were used to calculate the binding free energy between *Bc*β-tubulin and Zox. Per-residue decomposition was performed to identify the residues that make major contributions to *Bc*β-tubulin and Zox binding affinity. Our study provides a comprehensive molecular insight into the binding mechanism of *Bc*β-tubulin and Zox, and gives an explanation for the reduced sensitivity of mutated *Bc*β-tubulin to Zox at atomic level. Moreover, such information would provide theoretical support for further development of novel *Bc*β-tubulin inhibitor for the control of gray mold.

Methods

Preparing the structure of Bcβ-tubulin and zox

Due to the three dimensional structure of *Bc*β-tubulin has not been determined yet, the 3D structure of *Bc*β-tubulin was constructed by homology modeling. The sequence of *Bc*β-tubulin (accession number: AAB60307.1) was downloaded from the National Center for Biotechnology Information (NCBI). Based on the blast result, β-tubulin (PDB ID: 3N2G) (Barbier et al., 2010) was selected as a template for homology modeling (protein sequence identity = 82.47%). D chain of 3N2G was selected as template for it bound with an β-tubulin inhibitor G2N (ethyl [(2R)-5-amino-2-methyl-3-phenyl-1,2-dihydropyrido[3,4-b]pyrazin-7-yl]carbamate) and it has more complete secondary structure. The structure of G2N is similar to Zox. Its binding pocket in 3N2G overlaps with resistance sites of benzimidazoles. The template was downloaded from the Protein Date Bank, in which the small molecules and another chains were removed and only the D-chain was kept. The homology modeling is performed by MODELLER. The constructed model was subsequently minimized by Amber 14, with the force field of FF14SB. Based on the minimized wild type structure of β-tubulin, the mutations of β-tubulin^{F200Y} and β-tubulin^{M233I} were built respectively.

The structure of zoxamide was downloaded from PubChem Database. The 3D structure of zoxamide was optimized by Gaussian 09 program. The General Amber Force Field (GAFF) of Antechamber program from Amber 14 package was used to generate the parameter of zoxamide.

Molecular docking

Zox was docked to the binding pocket of wild type of *Bc*β-tubulin, which was accomplished by using the Autodock Vina program. The ligand and proteins were prepared by Autodock Tools (ADT), in which the water molecules were deleted, the polar hydrogen atoms were added and the atom charges were assigned. The grid center was set as the mass center of residues, Phe200, Met233 and Cys239 in *Bc*β-tubulin, which was calculated by VMD. We set searching space size to 15 Å. The exhaustiveness of global search algorithm was set to 50. The maximum energy difference between the best one and the lowest one was set to 5 (kcal/mol). We selected pose relying on the vina score and the comparison with the position of ligand, (G2N) in 3N2G. Zox was placed in the pocket of β-tubulin mutants by superimposing their structures to the wild type. Eventually, the complexes of β-tubulin^{WT}-Zox, β-tubulin^{F200Y}-Zox and β-tubulin^{M233I}-Zox were acquired.

Molecular dynamics simulations

According to the molecular docking results, the systems of β-tubulin^{WT}-*apo*, β-tubulin^{WT}-Zox, β-tubulin^{F200Y}-Zox and β-tubulin^{M233I}-Zox were subjected to molecular dynamics simulations in Amber 14 with the GPU parallel program. The parameter of protein was generated using the Amber FF14SB force field. On the basis of parameters of protein and ligand, three complex systems were assembled, in which the TIP3P water model was used, and the electric charge of whole system was neutralized with Na^+ ions. The H++ server was used to predict the pKa value of ionized residue, in which pH8 was selected as the condition of protonation state that based on experimental conditions (Banno et al., 2008).

The energy minimization of β-tubulin^{WT}-*apo*, β-tubulin^{WT}-Zox, β-tubulin^{F200Y}-Zox and β-tubulin^{M233I}-Zox systems were performed in three steps, respectively. To begin with, 5000 time step energy minimization was performed with a harmonic restraint of 5 kcal/mol·Å^{-2} applied on the whole protein and Zox. Then the backbone atoms of protein and heavy atoms of Zox were restrained for 5000 time steps energy minimization. The constraint was removed for the last 5000 time steps energy minimization. Each system was subsequently heated from 0 to 300 K gradually within 100 ps by restraining the backbone atoms and the heavy atoms of Zox under NVT ensemble. Then, the systems were relaxed under the NPT ensemble. The restraint was set as 5.0, 2.0, 1.0, 0.5, 0 kcal/mol·Å^{-2} within 1 ns. Molecular dynamics simulation of four systems was carried out within 100 ns. The SHAKE algorithm was employed to restrain the covalent bond involved with hydrogen atom. The particle grid Ewald (PME) method was applied to calculate the long-range electrostatic interaction. We select a 10.0 Å cut-off to calculate the van der waals interaction. The time step was set as 2 fs. The coordinate of each system was saved every 10 ps, which was used for trajectory analysis.

Analyzing residue interaction network

The representative structures derived from the MD trajectory of 80–100 ns in each system were used to construct the Residue Interaction Network (RIN). The interaction between amino acid residues and ligand was analyzed by the RINalyzer. The network of three systems was visualized with the software of Cytoscape and the plugin RINalyzer, in which the nodes and edges represent the residues or ligands and the non-covalent interactions with the residue-residue or residue-ligand, respectively.

Predicting binding free energy of complex systems

Based on the results of molecular dynamics simulation, the snapshots within 80–100 ns with 50 ps intervals were extracted from each system. All of the explicit water molecules were deleted. The 400 snapshots of each system were used to compute the binding free energy by MM-PBSA (Molecular Mechanics Poisson-Boltzmann Surface Area) and MM-GBSA (Molecular Mechanics Generalized Born Surface Area) method. The total binding free energy of the complex systems and the energy contribution of amino acids were calculated.

The total binding free energy in each system was evaluated according to the following formula:

$$\Delta G_{binding} = G_{complex} - G_{protein} - G_{Zox} \quad (1)$$

$G_{complex}$, $G_{protein}$ and G_{Zox} represent the free energy of complex, protein (β-tubulin^{WT}, β-tubulin^{F200Y} or β-tubulin^{M233I}), and Zox, respectively.

$$G = \Delta E_{MM} + \Delta G_{GB/PB} + \Delta G_{SA} - T\Delta S \quad (2)$$

$$\Delta E_{MM} = \Delta E_{ele} + \Delta E_{vdw} + \Delta E_{int} \quad (3)$$

$$\Delta G_{SA} = \gamma^{*}\Delta A + \beta \quad (4)$$

$$SE = \frac{STD}{\sqrt{N}} \quad (5)$$

Where ΔE_{MM} represents molecular mechanical (MM) energy of the molecule, which is the sum of the electrostatic energy (ΔE_{ele}), van der waals (ΔE_{vdw}) and internal energy (ΔE_{int}). The polar solvation energy ($\Delta G_{GB/PB}$), can be calculated by the Generalized Boltzmann (GB) or Poisson-Boltzmann (PB) equation. The dielectric constant for solvent was set to 80 and for solute was set to 1. The contribution of non-polar desolvation energy (ΔG_{SA}) was estimated by Equation (4). Thereinto, the surface tension proportionality constant (γ) and the free energy of non-polar solvation for a point solute (β) values were set to 0.0072 kcal/mol·Å^2 and 0.00, respectively in GB method and 0.00542 kcal/mol·Å^2 and 0.92 kcal/mol, respectively in PB method, respectively. ΔA represents the change of the solvent-accessible surface area (SASA) of the complex system, which was calculated by the LCPO algorithm. The $T\Delta S$ (vibrational entropy) is the change in the conformational entropy upon Zox binding, which is not calculated in our study for saving computational resources. The SE (standard errors) was calculated using Equation (5), in which STD and N are the standard deviation and the number of representative structures used in the calculation, respectively.

The MM-GBSA method was used to find the individual residue contribution to the total binding free energy between β-tubulin and Zox. Owning to its characteristic of high effectiveness and powerful ranking ability in calculating binding free energies, the MM-GBSA method was widely used to explore the interaction mechanism between drugs and their targets (Du, Qian, Yao, & Xue, 2019). The binding free energy contribution of each residue includes four terms: van der Waals contribution (ΔE_{vdw}), electrostatic contribution (ΔE_{ele}), polar solvation contribution (ΔG_{GB}) and nonpolar solvation contribution (ΔG_{SA}), without consideration the contribution of entropies.

Results and discussion

The interaction mode between Bcβ-tubulin and zox

The structure of *Bc*β-tubulin was predicted by homology modeling, which was shown in the Figure 1. We obtained the best model referred to the discrete optimized protein energy (DOPE) score of MODELLER. According to the interaction mode (Figure 2), it can be observed that Zox forms hydrogen bond interaction with Glu198 of *Bc*β-tubulin. It also forms hydrophobic interaction with residues including Ile4, Tyr50, Phe133, Ala165, Phe167, Phe/Tyr200, Val236, Leu240, Leu250, Leu253, Met257, Phe266, Ile316 and Val368, and polar amino acid with Gln131, Gln134, Thr237, Ser248 and Ser314. The template used in our work is the same as the previous work (Cai et al., 2015). The docked pose is different from that in the previous work. In previous reports, Zox was docked into the pocket of 3N2G. The amino acids around the binding pockets of wild type and mutant systems were Gln134, Asn165, Phe167, Glu198, Phe/Tyr200, Met/Ile233, Cys239, Val349 and Thr351.

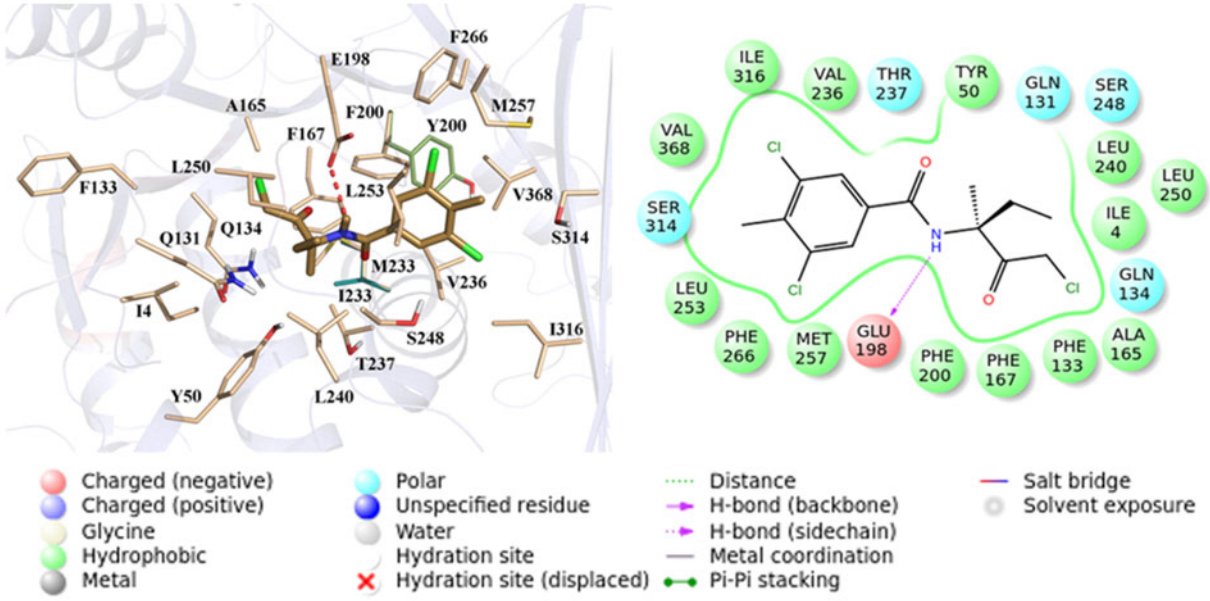

Figure 2. The interaction mode between β-tubulin^{WT}/β-tubulin^{F200Y}/β-tubulin^{M233I} and Zox. The carbon atoms of β-tubulin^{WT}, β-tubulin^{F200Y} and β-tubulin^{M233I} are colored in wheat, olive green and deepteal, respectively. The H atoms are omitted for clarity. The C, N, O, Cl atoms of Zox are colored in sand, blue, red and green, respectively.

Dynamics behavior of the wild type and mutant systems

The molecular dynamics simulation of β-tubulin^{WT}-*apo*, β-tubulin^{WT}-Zox, β-tubulin^{F200Y}-Zox and β-tubulin^{M233I}-Zox system was carried out within 100 ns. According to the MD trajectory, the molecular interaction between protein and ligand in complex system was explored and the resistance mechanism of mutant was explored further. In order to investigate the stability of each system and the overall convergence of MD trajectory, the Root Mean Square Deviation (RMSD) of the backbone atoms of β-tubulin was calculated, which was compared with the minimized structure. According to the degree of displacement of the backbone, the stability of each system was examined. From Figure 3, the β-tubulin^{WT}-*apo*, β-tubulin^{WT}-Zox, β-tubulin^{F200Y}-Zox and β-tubulin^{M233I}-Zox system reached equilibrium at 10 ns, 10 ns, 25 ns and 25 ns, respectively. The RMSD values of backbone atoms of β-tubulin converged at 2.07 ± 0.14, 2.23 ± 0.14, 2.12 ± 0.15 and 2.26 ± 0.21 Å in four systems. The RMSD values of zoxamide were substantially maintained at 1.17 ± 0.12, 1.67 ± 0.16 and 1.55 ± 0.20 Å in the β-tubulin^{WT}-Zox, β-tubulin^{F200Y}-Zox and β-tubulin^{M233I}-Zox system, respectively. In terms of the RMSDs, the four systems are overall stable, and the MD simulations are reliable. Thus, we took the last 20 ns simulation from each system for the following analyses.

The Root Mean Square Fluctuation (RMSF) versus residue number was calculated to measure the mobility of residues in entire MD simulations. According to the fluctuations of three systems, we found that the fluctuations occurred basically in the loop regions of β-tubulin, which was used to connect the secondary structures. According to the comparison of wild type to mutant systems (Figure 4), the loop regions of α1–α2, α10–β7, β7–α11 and α12–β9 exhibit

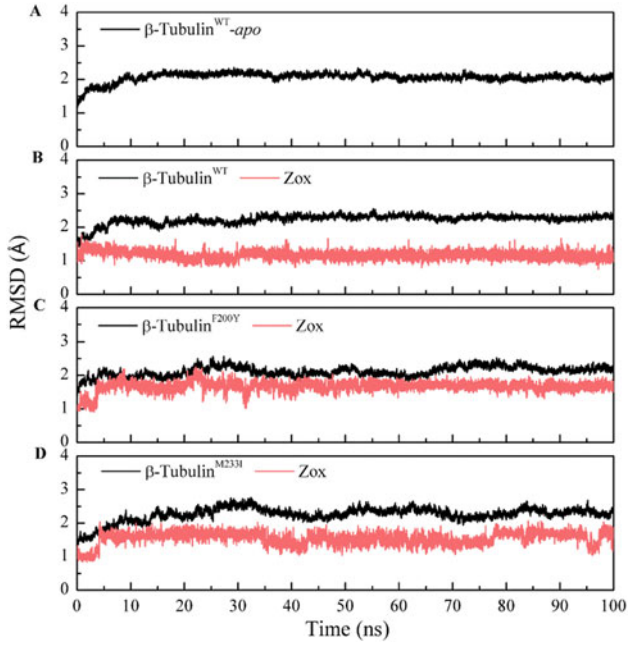

Figure 3. RMSD plots of the backbone atoms in complex system. (A) β-tubulin^{WT}-Zox system, (B) β-tubulin^{F200Y}-Zox system and (C) β-tubulin^{M233I}-Zox system.

higher flexibility relatively, which is related to the intrinsic flexibility of protein structure. The loop regions of β5–α8, α9, α9–α10 and α11–β8 show larger flexibility in β-tubulin^{F200Y}-Zox system than those in β-tubulin^{WT}-Zox system (Figure 4(A)). In the comparison of β-tubulin^{WT}-Zox and β-tubulin^{M233I}-Zox system (Figure 4(B)), the flexibility of β-tubulin^{WT} is larger than that of the β-tubulin^{M233I} in α3–α4, β3–α5 loop, while β5–α8, α9–α10 loop exhibit larger flexibility in β-tubulin^{M233I}-Zox system than those in β-tubulin^{WT}-Zox system.

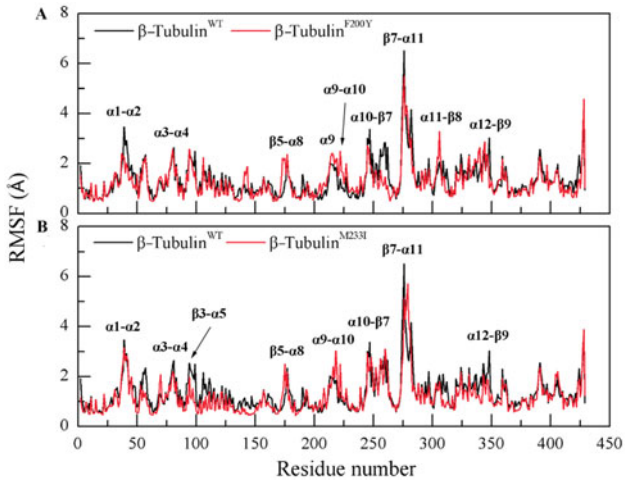

Figure 4. RMSF plots of Cα atoms of three systems. (A) Comparison of β-tubulin^{WT}-Zox and β-tubulin^{F200Y}-Zox system; (B) Comparison of β-tubulin^{WT}-Zox and β-tubulin^{M233I}-Zox system.

The comparison of binding mode of β-tubulin^{WT}-Zox with β-tubulin^{F200Y}-Zox, β-tubulin^{M233I}-Zox after MD simulation

For the sake of analyzing the interaction mode between Zox and β-tubulin in different system, the representative structures from 80 to 100 ns trajectory were extracted. When comes to interaction mode between protein and ligand, we can see the hydrogen bond interaction between Zox and Glu198 has disappeared in all the systems. The sidechain of Glu198 rotated and moved far away from Zox in the MD stage. The occupancy of the hydrogen bond with Glu198 in MD is not sufficient (Occupancy $<$ 13.86%), which indicated that this interaction is weak. As it shows in Figure 5(A), the hydroxyl of Tyr200 has a close contact with Zox in β-tubulin^{F200Y}-Zox, which makes Zox deflect compared with that in β-tubulin^{WT}-Zox system. Zox forms hydrophobic interaction with residues in β-tubulin^{F200Y} (Figure 5(A)), including Ile4, Tyr50, Met163, Ala165, Phe167, Tyr200, Val236, Cys239, Leu240, Leu246, Leu250, Ile316, Val368 and polar residues with Gln134, Thr237, Ser314, Gln350. The conformation of Arg251 exhibits obvious difference between β-tubulin^{WT} and β-tubulin^{F200Y}. In β-tubulin^{M233I}-Zox system, Zox forms hydrophobic interaction with residues in β-tubulin^{M233I} (Figure 5(B)), including Ile4, Phe133, Met163, Met164, Ala165, Phe167, Phe200, Val236, Cys239, Leu240, Leu246, Leu250, Leu253, Ala254, Met257, Ile316, and polar residues with Gln131, Gln134, Thr237, Ser314, Gln350.

Visual analysis of RIN in different systems

The interaction network of residues was used to understand the relationship of protein structure and function. Residue interaction network (RIN) has been applied to some aspects, which contains mutation effects, catalytic activity and so on (Xue, Wang, Jin, Liu, & Yao, 2012). In terms of interaction mode, zoxamide in wild type and mutant systems lost some interaction, at the same time novel interaction formed. We study the relationship between residues of β-tubulin and ligand zoxamide in different systems for understand the difference of binding mode on drug resistance.

The nodes and residue interaction network information about β-tubulin^{WT}-Zox, β-tubulin^{F200Y}-Zox and β-tubulin^{M233I}-Zox systems were generated and plotted (Figure 6). In wild type system, the network is the strongest (Figure 6(A)), in which there are 26 interactions between β-tubulin and zoxamide, including three van der waals interactions with Phe200, Cys239, Leu250 and 23 interactions between closest atoms. According to the networks of mutant systems, we can observe it relatively uncomplicated. There are 24 interactions between β-tubulin^{F200Y}-Zox with zoxamide, including two van der waals interactions with Ala165, Cys239 and 22 interactions between closest atoms (Figure 6(B)). In β-tubulin^{M233I}-Zox system, zoxamide forms 22 interactions with β-tubulin, including one van der waals interaction with Met163, and 21 interactions between closest atoms (Figure 6(C)).

On the degree of interaction network, the network in wild type system is obviously stronger than that of mutant systems. Therefore, the structure of wild type system is relatively more stable, while the conformational variation of β-tubulin in mutant systems weakens the interaction with zoxamide, which may lead to the reduced binding affinity.

The binding free energy between β-tubulin and zox

The binding free energy of β-tubulin^{WT}-Zox, β-tubulin^{F200Y}-Zox and β-tubulin^{M233I}-Zox system was calculated to conduct the quantitative estimation of wild type and mutant systems. As shown in Table 1, the contributions of electrostatic contributions (ΔE_{ele}), the van der waals contributions (ΔE_{vdw}), the polar solvation energy ($\Delta G_{GB/PB}$) to the total binding free energy are different in wild type and mutant systems. The detailed contribution of energy components were analyzed by MM-GBSA and MM-PBSA method. The electrostatic contribution (ΔE_{ele}) of wild type system (-6.31 ± 0.10 kcal/mol) is lower than β-tubulin^{F200Y}-Zox (-16.33 ± 0.15 kcal/mol) and β-tubulin^{M233I}-Zox (-10.66 ± 0.23 kcal/mol). The van der waals contribution (ΔE_{vdw}) of β-tubulin^{WT}-Zox (-45.86 ± 0.10 kcal/mol) is higher than β-tubulin^{F200Y}-Zox (-40.44 ± 0.10 kcal/mol) and β-tubulin^{M233I}-Zox (-37.37 ± 0.11 kcal/mol). The polar solvation energy ($\Delta G_{GB}/_{PB}$) contribution to the total binding free energy of β-tubulin^{WT}-Zox is 17.28 ± 0.10 kcal/mol for the MM-GBSA method, and 30.61 ± 0.17 kcal/mol for the MM-PBSA method compared to β-tubulin^{F200Y}-Zox (26.07 ± 0.14 kcal/mol, 38.84 ± 0.20 kcal/mol), and β-tubulin^{M233I}-Zox (22.13 ± 0.23 kcal/mol, 36.78 ± 0.31 kcal/mol), in which the former is lower than the latter, respectively. The non-polar solvation energy (ΔG_{SA}) shows little difference in three complex systems in both methods.

On the basis of the different interactions energy of estimating by the MM-GBSA method, the binding free energy (ΔG_{bind}) between β-tubulin and Zox in wild type system is lower than the mutant systems, with β-tubulin^{WT}-Zox (-28.60 ± 0.13 kcal/mol) $<$ β-tubulin^{F200Y}-Zox (-24.3 ± 0.12 kcal/mol) and β-tubulin^{WT}-Zox (-28.60 ± 0.13 kcal/mol) $<$ β-tubulin^{M233I}-Zox (-18.42 ± 0.12 kcal/mol). For the MM-PBSA

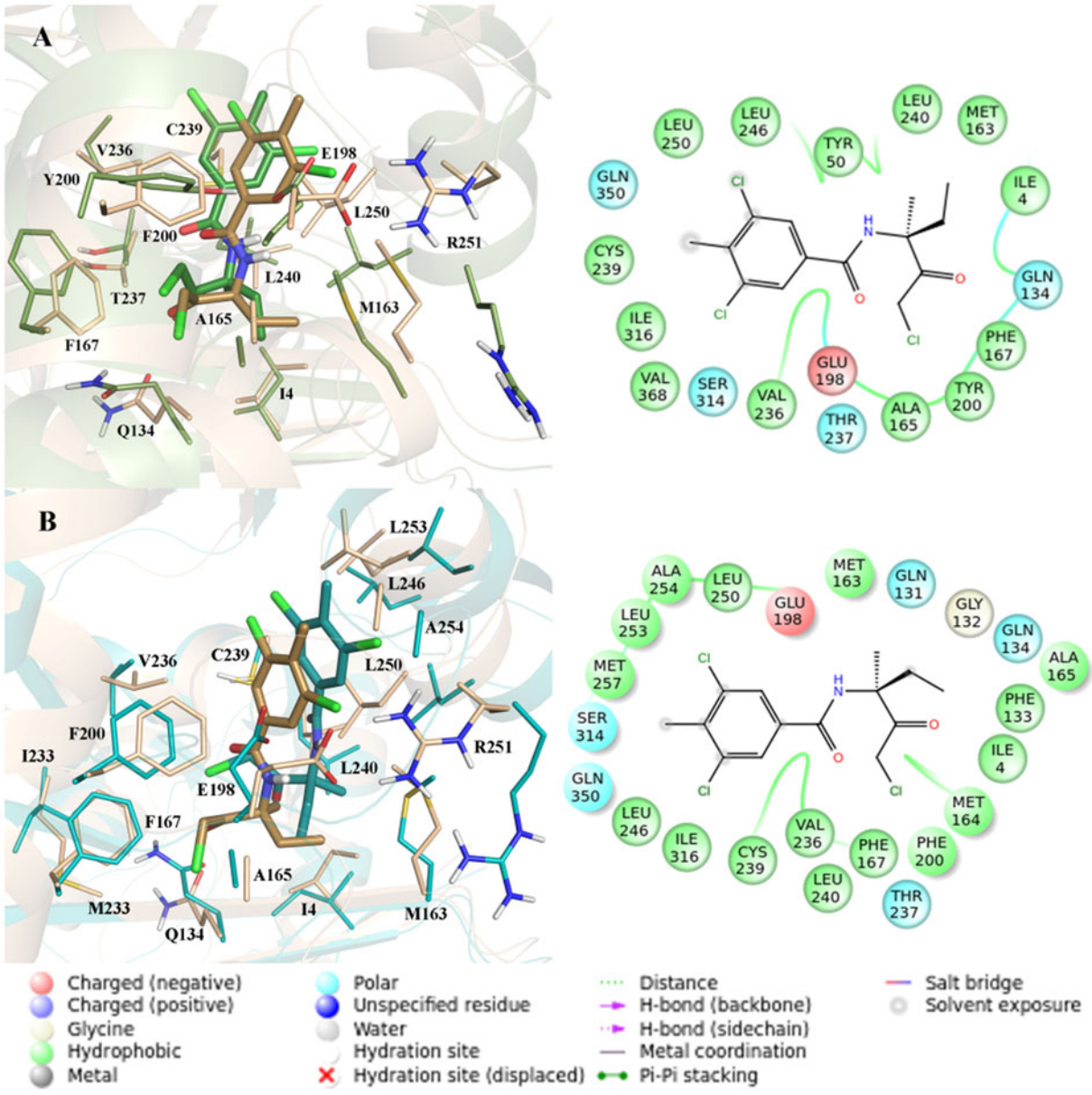

Figure 5. The representative structure of β-tubulin^{F200Y}-Zox, β-tubulin^{M233I}-Zox and β-tubulin^{WT}-Zox system extracted from the last 20 ns of the molecular dynamics simulation. (A) Comparison between wild type (β-tubulin^{WT}-Zox) and β-tubulin^{F200Y}-Zox system. The carbon atoms of β-tubulin^{WT} and β-tubulin^{F200Y} were colored in wheat and olive green, and the carbon atoms of Zox were colored in sand and forest. (B) Comparison between wild type (β-tubulin^{WT}-Zox) and β-tubulin^{M233I}-Zox systems. The carbon atoms of β-tubulin^{M233I} were colored in teal and the carbon atoms of Zox were colored in deepteal.

method, the binding free energy (ΔG_{bind}) between β-tubulin and Zox in wild type system is -25.22 ± 0.15 kcal/mol, lower than that in β-tubulin^{F200Y} (-22.02 ± 0.18) or β-tubulin^{M233I} (-15.23 ± 0.18) system. It suggests that the binding of β-tubulin and Zox is less strong in the two mutant systems than that in wild type system. The decreased binding affinity between mutant forms of β-tubulin and Zox may lead to high median effect concentration (EC_{50}) of the Zox to the mutant type, which is consistent with the reported work (Banno et al., 2008; Cai et al., 2015) that the EC_{50} values of the zoxamide-resistance isolates is larger than that of the zoxamide-sensitive isolates. It is indicated that the decreased binding affinity of Zox with two mutant forms of β-tubulin may result to the insensitivity of *Botrytis cinerea* to Zox. The components of binding free energy in Table 1 showed the major number of advantageous contributions for β-tubulin and Zox binding are ΔE_{ele} and ΔE_{vdw}, whereas the disadvantageous contributions for binding is the polar solvation energy.

Identification the key residues attributed to the total binding free energy

In order to quantitative interpretation the binding affinity more precisely, the decomposition of total binding free energy was performed, which is displayed in Figure 7. The MM-GBSA approach was used to calculate the contribution of per-residue in wild type and two mutant systems.

The distinction of energy contribution associated residues in wild type and two mutants were compared, respectively. The residues with energy contribution higher than |0.9| kcal/

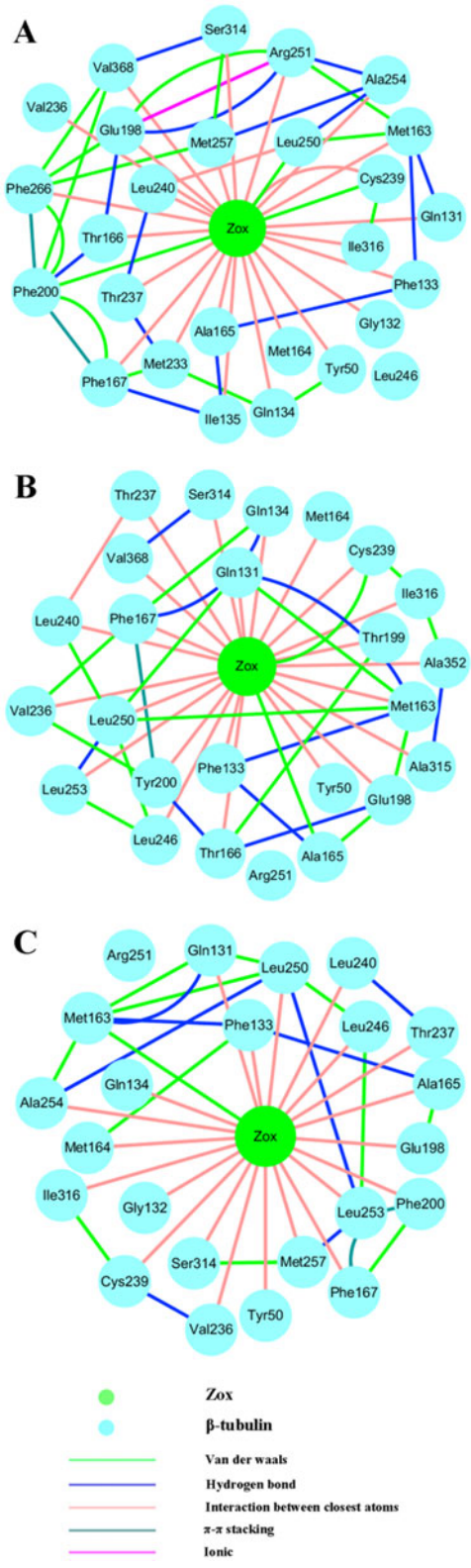

Figure 6. The residues interaction network of Zox binding with β-tubulin in wild type and mutant systems within 5 Å. (A) The residues interaction network of β-tubulin^{WT}-Zox system; (B) The residues interaction network of β-tubulin^{F200Y}-Zox system; (C) The residues interaction network of β-tubulin^{M233I}-Zox system. The edges were colored in accordance with their interaction type.

mol were shown in Figure 7. There are six residues in β-tubulin^{WT}-Zox, including Gln134 (−1.38 kcal/mol), Met163 (−0.91 kcal/mol), Ala165 (−0.94 kcal/mol), Phe200 (−2.36 kcal/

Table 1. Binding free energy for Zox bound to Bcβ-tubulin by MM-GB/PBSA methods.[a]

System	ΔE_{ele}	ΔE_{vdw}	ΔG_{SA}	ΔG_{GB}	ΔG_{bind}	ΔG_{SA}	ΔG_{PB}	ΔG_{bind}
β-Tubulin^{WT}-Zox	−6.31	−45.86	−5.84	17.28	−28.60	−5.16	30.61	−25.22
	±0.10	±0.10	±0.01	±0.10	±0.13	±0.01	±0.17	±0.15
β-Tubulin^{F200Y}-Zox	−16.33	−40.44	−5.37	26.07	−24.3	−5.25	38.84	−22.02
	±0.15	±0.10	±0.01	±0.14	±0.12	±0.005	±0.20	±0.18
β-Tubulin^{M233I}-Zox	−10.66	−37.37	−5.01	22.13	−18.42	−5.19	36.78	−15.23
	±0.23	±0.11	±0.01	±0.23	±0.12	±0.005	±0.31	±0.18

[a]All energies are in kcal/mol.

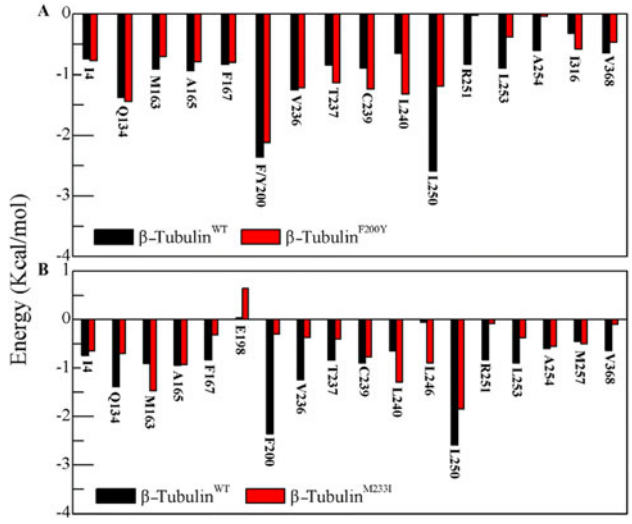

Figure 7. Per-residue energy contribution plots. (A) Comparison between wild type (β-tubulin^{WT}-Zox) and β-tubulin^{F200Y}-Zox systems of per-residue energy contributions; (B) Comparison between wild type (β-tubulin^{WT}-Zox) and β-tubulin^{M233I}-Zox systems of per-residue energy contributions.

mol), Val236 (−1.25 kcal/mol) and Leu250 (−2.59 kcal/mol). There are seven residues with high contribution in β-tubulin^{F200Y}-Zox system, such as Gln134 (−1.44 kcal/mol), Tyr200 (−2.12 kcal/mol), Val236 (−1.22 kcal/mol), Thr237 (−1.13 kcal/mol), Cys239 (−1.24 kcal/mol), Leu240 (−1.32 kcal/mol) and Leu250 (−1.19 kcal/mol) (Figure 7(A)). For β-tubulin^{M233I}-Zox system, there are five residues, including Met163 (−1.47 kcal/mol), Ala165 (−0.93 kcal/mol), Leu240 (−1.29 kcal/mol), Leu246 (−0.9 kcal/mol) and Leu250 (−1.84 kcal/mol) (Figure 7(B)). The positional relationship between these residues and zoxamide was shown in the Figure 5, in which we can observe that these residues are close to Zox in each system.

The residues with large energy contribution in two mutant systems are different from the wild type system. Therefore, we identified the major residues with significant energy difference between wild type and mutant systems. By comparison, these residues in wild type system revealed remarkably larger energy contribution than those in β-tubulin^{F200Y}-Zox system, including Leu250 ($|\Delta| = 1.4$ kcal/mol) and Arg251 ($|\Delta| = 0.81$ kcal/mol), which are located at α10–β7 loop. The loop region changed with greater flexibility in the wild type than in mutant systems, which may be beneficial to the change of residue conformation in the direction of interaction with Zox. Besides, Leu240 ($|\Delta| = 0.67$ kcal/mol) provides more beneficial contribution in β-tubulin^{F200Y}-Zox system than those in wild type system. In β-tubulin^{WT}-Zox system, Leu250 is closer to the Zox than it

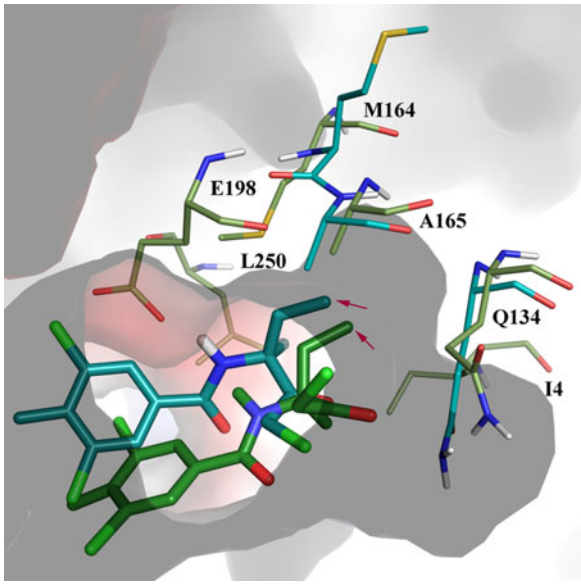

Figure 8. The electrostatic surface representation of Βcβ-tubulin and Zox. The carbon atoms of β-tubulin^{F200Y}-Zox and β-tubulin^{M233I}-Zox system were colored in olive green and teal, and the carbon atoms of Zox were colored in forest and deepteal.

in β-tubulin^{F200Y}-Zox system, and formed van der waals interaction with Zox (Figure 6(A)). This interaction disappeared in β-tubulin^{F200Y}-Zox system (Figure 6(B)). The side chain of Arg251 rotated to Zox in wild type system, while the side chain of Arg251 moves far from Zox in β-tubulin^{F200Y}-Zox system (Figure 5(A)). Arg251 interacts with Zox to form interaction between closest atoms in wild type system (Figure 6(A)), while in β-tubulin^{F200Y}-Zox system, this interaction disappeared due to conformational change (Figure 6(B)). The position of Leu240 is closer to Zox in β-tubulin^{F200Y}-Zox system than in β-tubulin^{WT}-Zox system. The change of conformation and the weakening of interactions explain why the contribution of the same residue is obvious difference in two systems.

In β-tubulin^{M233I}-Zox system, there are five residues exhibited dramatically lower energy contribution than those in β-tubulin^{WT}-Zox system, which contain Gln134 ($|\Delta| = 0.68$ kcal/mol), Phe200 ($|\Delta| = 2.06$ kcal/mol), Val236 ($|\Delta| = 0.88$ kcal/mol), Leu250 ($|\Delta| = 0.75$ kcal/mol) and Arg251 ($|\Delta| = 0.75$ kcal/mol). There are two residues exhibited increased energy contribution in β-tubulin^{M233I}-Zox system, including Leu240 ($|\Delta| = 0.64$ kcal/mol), and Leu246 ($|\Delta| = 0.85$ kcal/mol). From the interaction mode (Figure 5(B)), we can see that the positions of Gln134, Phe200, Val236, Leu250 and Arg251 in β-tubulin^{WT}-Zox system are closer to Zox than those in β-tubulin^{M233I}-Zox system. Among the residues with high energy contribution, Phe200 and Arg250 formed van der waals interaction with Zox in wild type system (Figure 6(A)), while these interaction disappeared and interaction between closest atoms formed in β-tubulin^{M233I}-Zox system (Figure 6(C)). Leu240 moves closer to Zox in β-tubulin^{M233I}-Zox compared to β-tubulin^{WT}-Zox system, which contributes more to the total binding free energy. Leu246 moves closer to Zox because of the conformational change of loop region (α10–β7), and interacts with Zox to form new molecular interaction in β-tubulin^{M233I}-Zox system (Figure 6(C)). Residues, Gln134, Phe200, Val236, Leu250 and Arg251 interacting with Zox in mutant system mainly have undergone conformational change, which led to less spatial contact with zoxamide, weaker interaction and lower contribution to binding free energy further. These may not satisfy the requirement of β-tubulin sensitive to Zox.

In order to improve the binding affinity between Zox and β-tubulin mutants, the electrostatic surface of representative structure of two mutant systems was displayed to find out how to modify Zox (Figure 8). It is suggested that the substitution of larger groups for –CH3 group (red arrows), such as –CH(CH3)2 or –C(CH3)3 would make Zox occupy the hydrophobic pocket, forming more favorable hydrophobic interaction with residues Ile4, Gln134, Met163, Ala165 in β-tubulin^{F200Y}-Zox system and Gln134, Met164, Ala165 in β-tubulin^{M233I}-Zox system. The modification strategy, also suggested in the previous work of Young et al. (Michelotti & Young, 1992), would make Zox counteract the resistance.

Conclusion

In the present study, the interaction mode between *Bc*β-tubulin and Zox was explored by multiple computational methods including homology modeling, molecular docking, molecular dynamics simulations, residue interaction network, and binding free energy calculation. The interaction mode analyses based on the MD trajectories indicate that it is different between the wild type form of *Bc*β-tubulin and the mutation forms. The residue interaction network analysis, binding free energy calculation indicated that the interaction and binding free energy between Bcβ-tubulin and Zox is stronger in the wild type than that in the mutated forms (F200Y and M233I). In β-tubulin^{F200Y}-Zox system, the swing of Leu250 and Arg251 led to the looser interaction between β-tubulin^{F200Y} and Zox, which may result in the insensitivity of *Botrytis cinerea* to Zox. The conformational change of Gln134, Phe200, Val236, Leu250 and Arg251 led to unfavorable interaction and the reduced energy contribution to the binding between β-tubulin^{M233I} and Zox, which may contribute to the resistance against Zox. In summary, the results obtained in this study are benefit to understand the interaction mechanism between *Bc*β-tubulin and Zox, and provides valuable reference for future structure-based fungicide design.

Disclosure statement

No potential conflict of interest was reported by the authors.

Funding

This work was funded by the Natural Science Foundation of Shandong Province, China (Grant nos. ZR2018QB004; ZR2015CM017), the Shandong Provincial Key Research and Development Project (Grant no. 2016GSF117026), the Talents of High Level Scientific Research Foundation (Grant No. 6631113318) and the Graduate Research Plan (QYC201840) of Qingdao Agricultural University.

Author contributions

JD conceived and supervised the experiments. SJD performed MD simulations. SJD, KZ and JD analyzed the data. SJD, JD and XJY wrote the paper.

ORCID

Juan Du http://orcid.org/0000-0001-5993-4949

References

Adnan, M., Hamada, M. S., Li, G. Q., & Luo, C. X. (2018). Detection and molecular characterization of resistance to the dicarboximide and benzamide fungicides in Botrytis cinerea from tomato in Hubei Province. *Plant Disease*, *102*(7), 1299–1306. doi:10.1094/PDIS-10-17-1531-RE

Banno, S., Fukumori, F., Ichiishi, A., Okada, K., Uekusa, H., Kimura, M., & Fujimura, M. (2008). Genotyping of benzimidazole-resistant and dicarboximide-resistant mutations in Botrytis cinerea using real-time polymerase chain reaction assays. *Phytopathology*, *98*(4), 397–404. doi:10.1094/PHYTO-98-4-0397

Barbier, P., Dorléans, A., Devred, F., Sanz, L., Allegro, D., Alfonso, C., … Andreu, J. M. (2010). Stathmin and interfacial microtubule inhibitors recognize a naturally curved conformation of tubulin dimers. *Journal of Biological Chemistry*, *285*(41), 31672–31681. doi:10.1074/jbc.M110.141929

Cai, M., Lin, D., Chen, L., Bi, Y., Xiao, L., & Liu, X. L. (2015). M233I mutation in the β-tubulin of Botrytis cinerea confers resistance to zoxamide. *Scientific Reports*, *5*(1), 16881. doi:10.1038/srep16881

Dean, R., Van Kan, J. A. L., Pretorius, Z. A., Hammond-Kosack, K. E., DI Pietro, A., Spanu, P. D., … Foster, G. D. (2012). The top 10 fungal pathogens in molecular plant pathology. *Molecular Plant Pathology*, *13*(4), 414–430. doi:10.1111/j.1364-3703.2011.00783.x

Du, Q., Qian, Y., Yao, X. J., & Xue, W. W. (2019). Elucidating the tight-binding mechanism of two oral anticoagulants to factor Xa by using induced-fit docking and molecular dynamics simulation. *Journal of Biomolecular Structure and Dynamics*. Advance online publication. doi:10.1080/07391102.2019.1583605

Leroux, P., Fritz, R., Debieu, D., Albertini, C., Lanen, C., Bach, J., … Chapeland, F. (2002). Mechanisms of resistance to fungicides in field strains of Botrytis cinerea. *Pest Management Science*, *58*(9), 876–888. doi:10.1002/ps.566

Michelotti, E. L., & Young, D. H. (1992). U.S. Patent No. 5304572. Washington, DC: U.S. Patent and Trademark Office.

Negri, S., Lovato, A., Boscaini, F., Salvetti, E., Torriani, S., Commisso, M., … Guzzo, F. (2017). The induction of noble rot (Botrytis cinerea) infection during postharvest withering changes the metabolome of grapevine berries (Vitis vinifera L., cv. Garganega). *Frontiers in Plant Science*, *8*, 1002. doi:10.3389/fpls.2017.01002

Van Kan, J. A. L. (2006). Licensed to kill: The lifestyle of a necrotrophic plant pathogen. *Trends in Plant Science*, *11*(5), 247–253. doi:10.1016/j.tplants.2006.03.005

Wang, M., Du, Y., Liu, C., Yang, X., Qin, P., Qi, Z., … Li, X. (2019). Development of novel 2-substituted acylaminoethylsulfonamide derivatives as fungicides against Botrytis cinerea. *Bioorganic Chemistry*, *87*, 56–69. doi:10.1016/j.bioorg.2019.03.017

Wu, F. X., Wang, F., Yang, J. F., Jiang, W., Wang, M. Y., Jia, C. Y., … Yang, G. F. (2018). AIMMS suite: A web server dedicated for prediction of drug resistance on protein mutation. *Briefings in Bioinformatics*. Advance online publication. doi:10.1093/bib/bby113

Xue, W., Wang, M., Jin, X., Liu, H., & Yao, X. (2012). Understanding the structural and energetic basis of inhibitor and substrate bound to the hepatitis C virus full-length NS3/4A protease: Insights from molecular dynamics simulation, binding free energy calculation and network analysis. *Molecular Biosystems*, *8*(10), 2753–2765. doi:10.1039/c2mb25157d

Young, D. H., & Slawecki, R. A. (2001). Mode of action of zoxamide (RH-7281), a new oomycete fungicide. *Pesticide Biochemistry and Physiology*, *69*(2), 100–111. doi:10.1006/pest.2000.2529

Zhu, X. L., & Yang, G. F. (2012). A comparative study of drug resistance mechanism associated with active site and non-active site mutations: I388N and D425G mutants of acetyl-coenzyme-A carboxylase. *Current Computer Aided-Drug Design*, *8*(1), 62–69. doi:10.2174/157340912799218480